A&A 649, A135 (2021)
https://doi.org/10.1051/0004-6361/202140439

Astronomy & Astrophysics

The variable absorption in the X-ray spectrum of GRB 190114C

Sergio Campana[1], Davide Lazzati[2], Rosalba Perna[3,4], Maria Grazia Bernardini[1], and Lara Nava[1]

[1] INAF-Osservatorio Astronomico di Brera, Via E. Bianchi 46, 23807 Merate (LC), Italy
e-mail: sergio.campana@inaf.it
[2] Department of Physics, Oregon State University, 301 Weniger Hall, Corvallis, OR 97331, USA
[3] Department of Physics and Astronomy, Stony Brook University, Stony Brook, NY 11794-3800, USA
[4] Center for Computational Astrophysics, Flatiron Institute, New York, NY 10010, USA

Received 28 January 2021 / Accepted 7 March 2021

ABSTRACT

Gamma-ray burst (GRB) 190114C was a bright burst that occurred in the local Universe ($z = 0.425$). It was the first GRB ever detected at teraelectronvolt (TeV) energies, and this was thanks to MAGIC. We characterize the ambient medium properties of the host galaxy through the study of the absorbing X-ray column density. Using a combination of *Swift*, *XMM-Newton*, and *NuSTAR* observations, we find that the GRB X-ray spectrum is characterized by a high column density that is well in excess of the expected Milky Way value and decreases, by a factor of ∼2, around $\sim 10^5$ s. Such a variability is not common in GRBs. The most straightforward interpretation of the variability in terms of the photoionization of the ambient medium is not able to account for the decrease at such late times, when the source flux is less intense. Instead, we interpret the decrease as due to a clumped absorber, denser along the line of sight and surrounded by lower-density gas. After the detection at TeV energies of GRB 190114C, two other GRBs were promptly detected. These two also have high intrinsic column density values, and there are hints for a decrease in their column densities as well. We speculate that a high local column density might be a common ingredient of TeV-detected GRBs.

Key words. gamma-ray burst: general – gamma-ray burst: individual: GRB190114C – dust, extinction

1. Introduction

Since the early observations of gamma-ray bursts (GRBs), it has been recognized that the study of their immediate environment plays a very important role in gaining a more complete understanding of the properties of their progenitors (e.g., Mirabal et al. 2003; Fryer et al. 2006; D'Elia et al. 2007, 2009; Hjorth et al. 2012; Krühler et al. 2015; Vergani et al. 2015; Perley et al. 2016).

For example, low density environments, typical of the outer regions of galaxies, are preferentially expected in association with long-lived progenitors, such as compact object binaries, due to their generally long merging times (e.g., Berger et al. 2005; Belczynski et al. 2006). This is characteristic of short GRBs. On the other hand, GRBs associated with the collapse of massive stars (such as the long GRBs; Stanek et al. 2003; Hjorth et al. 2003) are expected to occur within star forming regions, which is thus reflected in the higher densities of the circumburst medium. Even more informative, when it can be inferred from the data, is the density profile in the immediate vicinity of the source since this carries information on the last stages of the life of a massive star, such as the extent and amount of mass lost in a wind or the presence of shells of material ejected prior to the GRB (Racusin et al. 2008), as expected in a two-step explosion (Vietri & Stella 1998).

Several proposals for the origin of the X-ray absorption in excess of the Galactic value in GRBs have been suggested, both in individual sources as well as from a sample perspective. The easiest explanation involves material in the host galaxy, either local to the GRB (Galama & Wijers 2001; Stratta et al. 2004; Gendre et al. 2006; Schady et al. 2007; Campana et al. 2012) or on a more extended basis (HII regions, Watson et al. 2013; molecular clouds, Reichart & Price 2002; Campana et al. 2006). Another possibility involves the metal contribution from the intergalactic medium (IGM) along the line of site (Behar et al. 2011; Starling et al. 2013; Campana et al. 2015; Dalton & Morris 2020). These possibilities are not mutually exclusive.

One way to probe the properties of the absorbing medium is via time-resolved measurements of the column density of the absorbing material along the line of sight from the observer to the source, $N_{\rm H}$. If time variability in the absorption is observed, it can yield powerful information on the immediate environment of the source.

The long gamma-ray burst GRB 190114C, which triggered both the *Neil Gehrels Swift* Observatory and the *Fermi* satellite on January 14, 2019 (Gropp et al. 2019; Ajello et al. 2020), was followed by an extensive observational campaign at various wavelengths due to its high luminosity ($E_{\gamma,\rm iso} = (2.5 \pm 0.1) \times 10^{53}$ erg) and relatively low redshift ($z = 0.425$, Selsing et al. 2019), making the burst extremely bright (MAGIC Collaboration 2019a). The closeness of the GRB makes the IGM contribution negligible (e.g., Arcodia et al. 2018). In addition, the optical absorption is high $E(B-V) \sim 0.83$, supporting the evidence for a high intrinsic absorption (de Ugarte Postigo et al. 2020). Remarkably, observations by the MAGIC collaboration also revealed teraelectronvolt (TeV) emission, a first for a GRB (MAGIC Collaboration 2019b).

Here we present X-ray observations of GRB 190114C with the *Swift* X-ray Telescope (XRT), from the earliest observation time window (starting 68 s after the burst) to the latest afterglow observations, on a timescale of ∼10 days, together with long *XMM-Newton* and *NuSTAR* observations. During this period, the effective column density, $N_{\rm H}$, was observed to decline by approximately a factor of two.

Table 1. Log of the X-ray observations.

Telescope	Obs. ID	Start time (2019-)	Expos. (s)
Swift/XRT	00883832000	01–14 20:39:00	558.9
Swift/XRT	00883832001	01–14 21:55:36	19412.5
Swift/XRT	00883832002	01–15 14:18:35	7454.2
Swift/XRT	00883832003	01–16 02:44:35	2788.1
Swift/XRT	00883832004	01–16 09:10:34	2419.5
Swift/XRT	00883832005	01–17 05:57:36	2392.0
Swift/XRT	00883832006	01–17 09:06:35	2725.4
Swift/XRT	00883832007	01–18 05:45:34	4974.5
Swift/XRT	00883832008	01–19 12:05:35	3582.9
Swift/XRT	00883832009	01–20 13:31:34	4681.1
Swift/XRT	00883832010	01–21 16:46:35	3066.4
Swift/XRT	00883832012	01–22 02:19:51	4979.5
XMM-Newton	0729161101	01–15 05:12:01	35421.9
XMM-Newton	0729161201	01–24 06:17:08	10838.0
NuSTAR	90501602002	01–15 19:16:09	52391.2

The most natural explanation for a decline in $N_{\rm H}$ during the time that the source was active is photoionization of the medium along the line of sight to the observer by the strong X-ray and UV radiation accompanying the burst. As the radiation propagates into the medium, it gradually photoionizes it, hence reducing the opacity of the medium encountered by the later radiation front. This phenomenon can result in time-dependent absorption lines – and has been discussed in both the optical (Perna & Loeb 1998; Mirabal et al. 2002; Dessauges-Zavadsky et al. 2006; Thöne et al. 2011) and the X-ray bands (Böttcher et al. 1999; Lazzati et al. 2001) – as well as more generally for the effective column density, $N_{\rm H}$, which is an integral quantity typically measured in X-ray spectral fits (Frontera et al. 2004; Campana et al. 2007; Grupe et al. 2010). Whether the variability is appreciable enough to be measurable in time-resolved spectra depends on both the brightness of the source and on the radial extent of the absorbing medium. GRB 190114C fulfills these conditions and, with its measured variability in $N_{\rm H}$, offers us an opportunity to probe the environment in the immediate vicinity of the source.

This paper is organized as follows: Sect. 2 presents the X-ray data and the time-resolved spectral fits, leading to the measurements of the variable $N_{\rm H}$. In Sect. 3 we perform a detailed statistical analysis aimed at determining whether time-dependent photoionization of the line-of-sight absorbing medium can provide a reasonable fit to the data for $N_{\rm H}(t)$. The large χ^2 of the best fit leads us to conclude that this is not a likely explanation for the observed variability. In Sect. 4 we suggest some alternative explanations. In particular, we show that an absorber with a low surface filling fraction can reproduce the observed variability, at least qualitatively. We summarize and conclude our work in Sect. 5.

2. X-ray data and light curve modeling

The *Neil Gehrels Swift* Observatory (Gehrels et al. 2004), after the detection of the GRB with the Burst Alert Telescope (BAT; Gropp et al. 2019), autonomously re-pointed its narrow field instruments and the XRT started observing 68 s after the event. When XRT started observing, BAT was still collecting useful data, allowing for a 130 s superposition. *Swift*/XRT observed the GRB for about a month with 26 exposures. Useful spectral data stop at ∼11 d. Together with *Swift*, GRB 190114C has been observed once by *NuSTAR* and twice by *XMM-Newton*. A log of all the X-ray observations can be found in Table 1.

Swift/XRT collected data in windowed timing (WT) mode up to ∼5000 s from the burst, testifying to the burst brightness. The spectra from these WT data were extracted, with only single pixel events selected in order to increase the spectral resolution and minimize the effects of charge redistribution at low energies. We also used the new analysis software included in `HEASOFT` v.6.26 to minimize the effects of charge trapping. These data were extracted manually. To extend the XRT spectral range, we also extracted BAT data up to ∼200 s. We analyzed *Swift*/BAT data and processed them with the standard *Swift* analysis software included in `HEASOFT` v.6.26 and the relevant calibration files. We extracted 15−150 keV BAT spectra and response matrices with the `batbinevt` and `batdrmgen` tasks in FTOOLS in two time intervals: 68−132 s and 132−196 s. Beyond this time there was not sufficient signal to extract a spectrum.

All the other XRT data were collected in photon counting (PC) mode. These XRT spectra were extracted using the Leicester University tools[1] and automatically correcting for all the instrumental features (Evans et al. 2009). For all the spectra, we retained data in the 0.3–10 keV energy range and standard grade selection (1–12). We binned the spectra to one photon per energy channel to allow for the use of C-statistics.

The first *XMM-Newton* observation started 8.3 h after the burst. Data were processed following standard filtering criteria according to *XMM-Newton* threads[2]. The net exposure time was 35 ks. Given the high count rate, we retained the pn data only. Source data were extracted from an 800-pixel region, and the background from a close-by region free of sources and of a 1000-pixel radius. The second observation started 9.4 d after the event. The count rate was lower by a factor of ∼100, so we retained all the three European Photon Imaging Cameras (EPICs). Due to the high background, we filtered the data with a pn threshold of 0.8 counts s^{-1}. The net exposures were 10.8, 9.3, and 9.3 ks for the pn, MOS1, and MOS2, respectively. As it was the weaker source, we extracted photons from a 400-pixel radius region. We retained data in the 0.3–10 keV energy range. We binned the data to one photon per energy channel.

The *NuSTAR* observation took place 22.4 h after the burst. We started from the standard cleaned data, grouping the three event files for each instrument. We extracted the spectra from a region of 49″ radius centered on source. The background was extracted from a circular region of 109″ radius. We considered data in the 3–60 keV energy range and binned the data to one photon per energy channel.

We divided the data into ten time slices (see Table 2). Spectra were fitted with `XSPEC` (v12.11.1), and we adopted C-statistics (Cash 1979). Although the collected data span a large time interval (68 s – 10 d) and we are dealing with a large wealth of data, we adopted a simplistic spectral model: two smoothly joined power laws (`sbpl` in `XSPEC`) with Galactic and intrinsic absorption, modeled with `tbabs`. The Galactic absorption was fixed to 7.45×10^{19} cm^{-2} (Willingale et al. 2013). The intrinsic column density was evaluated at the GRB redshift ($z = 0.425$) and left free to vary from one time slice to another. The two power law indices were tied together among all observations, and only the peak energy was free to vary. The smoothness parameter was

[1] https://www.swift.ac.uk/xrt_spectra/
[2] https://www.cosmos.esa.int/web/xmm-newton/sas-threads

Table 2. Time slices used for spectral analysis.

Number	Time slice (s)	Instrument	$N_{\rm H}(z)$ (10^{22} cm^{-2})	$E_{\rm peak}$ (keV)
1	67.7–132	BAT – XRT (WT grade 0)	$8.79^{+0.57}_{-0.68}$	$15.2^{+13.7}_{-10.5}$
2	132–196	BAT – XRT (WT grade 0)	$8.94^{+0.75}_{-0.59}$	$41.5^{+53.2}_{-22.1}$
3	196–644	XRT (WT grade 0)	$8.06^{+0.39}_{-0.65}$	>37.5
4	3844–4164	XRT (WT grade 0)	$8.86^{+0.80}_{-1.12}$	<6.7
5	5507–9988	XRT (PC)	$8.02^{+1.51}_{-1.23}$	>4.7
6	9988–29315	XRT (PC)	$7.38^{+0.77}_{-0.76}$	>8.2
7	32515–80900	XMM (pn) – XRT (PC)	$6.50^{+0.17}_{-0.26}$	$13.8^{+14.6}_{-4.3}$
8	80644–142660	*NuSTAR* (A+B) – XRT (PC)	$7.75^{+1.33}_{-1.19}$	$7.1^{+7.2}_{-5.6}$
9	205508–769284	XRT (PC)	$4.25^{+2.41}_{-1.27}$	–
10	811350–855900	XMM (pn+MOS1+MOS2)	$4.26^{+0.72}_{-0.83}$	$4.3^{+0.6}_{-0.5}$

Notes. Errors are at the 90% confidence level for one parameter of interest.

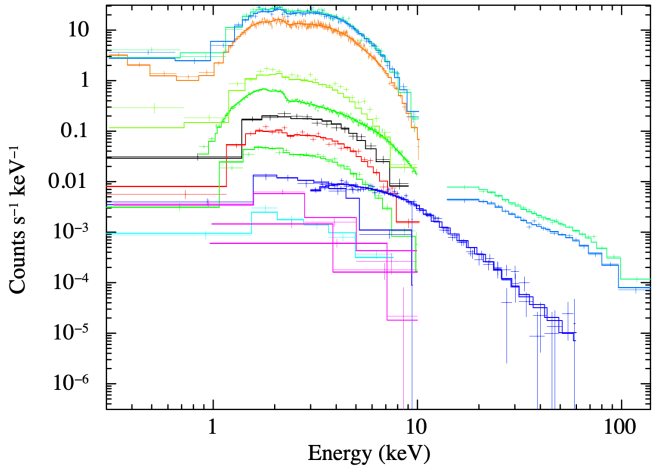

Fig. 1. Fit of the spectral data. Data were heavily re-binned for display purposes. From top to bottom, spectra are shown in order of increasing time and decreasing flux. Spectra, as numbered in Table 2, are plotted in green and cyan (1), blue and cyan (2), orange (3), yellow and green (4), black (5), red (6), green (7), blue (8), light blue (9), and magenta (10).

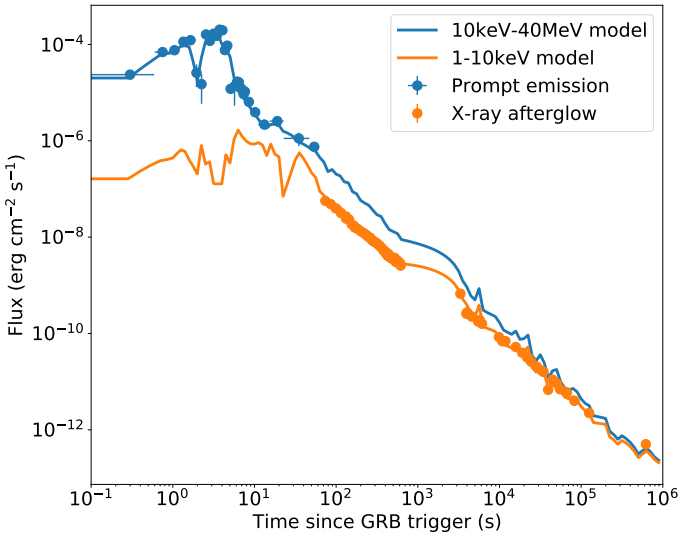

Fig. 2. Comparison between the prompt and X-ray afterglow observations of GRB 190114C with the model light curve and spectral evolution adopted in the photoionization code. The prompt emission data are from Ravasio et al. (2019); the afterglow data are from this work.

kept fixed to 1; we verified that this is a parameter that cannot be fitted and that results do not vary too much for other, different choices. A constant factor was added to cope with instrument calibration uncertainties, resulting in different values of the power law normalization. The same value of the constant was adopted for the same instrument. A value of 1 was kept for the *Swift*/XRT data taken in PC mode.

The overall fit is good, with a C-statistic of 6293.2 with 6850 degrees of freedom. The normalization constants are close to 1, as expected (see Fig. 1). The power law photon indices are $\alpha_1 = 1.47^{+0.18}_{-0.30}$ and $\alpha_2 = 2.14^{+0.19}_{-0.08}$ (errors were computed for $\Delta\chi^2 = 2.71$). These values of the photon indices are consistent with synchrotron radiation from a nonthermal electron population injected with spectral index $p \sim 2.2$. The intrinsic column density and the peak energy decrease with time (see Table 2). The decreasing peak energy (corresponding to the cooling energy) is suggestive of a constant density medium (Panaitescu & Kumar 2000). The initial intrinsic column density is very high, $\sim 9 \times 10^{23}$ cm^{-2} (the mean intrinsic column density for bright bursts is $\sim 5 \times 10^{21}$ cm^{-2}; Campana et al. 2012).

We extracted the GRB light curve from the *Swift*/XRT light curve repository and converted it into 1–10 keV flux (Fig. 2). For each spectral slice we computed the (variable) conversion factor from the XRT count rate to 1–10 keV unabsorbed flux. Then, we interpolated these conversion factors and converted all the count rates to the flux light curve shown in Fig. 2.

To reconstruct the 1–10 keV light curve before 70 s, we used the flux measured in the 10 keV–40 MeV band by Ravasio et al. (2019). The spectrum is assumed to be either a broken power law or a single power law, as requested by the fit.

As is apparent from Table 2, the column density, $N_{\rm H}$, decreases with time. A linear fit yields a $\chi^2 = 81.6$ with eight degrees of freedom, hence ruling out a linear decrease and calling for a different functional form for the measured variability. A possible fit involves a power law (with an index of 0.22) and a constant, yielding a $\chi^2 = 10.0$ with seven degrees of freedom. In the following, we explore physical models that can lead to a time-decreasing $N_{\rm H}$.

3. Modeling with time-dependent photo-absorption

The most natural explanation for the observed reduction in the column density to the source during the time of observation is photoionization by the strong UV and X-ray radiation (Perna & Lazzati 2002; Lazzati et al. 2001; Lazzati & Perna 2002). We thus here quantitatively explore whether this interpretation is supported by the data.

The GRB radiation source is assumed to turn on in a medium in thermal equilibrium at an initial temperature of $T_{\rm in} = 10^3$ K. The time-dependent photoionization of the medium is computed using the code developed by Perna & Lazzati (2002) and Perna et al. (2003) and described in detail in those papers. The code includes 13 elements, that is, hydrogen and the 12 most abundant astrophysical elements – He, C, N, O, Ne, Mg, Si, S, Ar, Ca, Fe, and Ni – with solar abundances. The ionic number densities of those elements are computed as a function of space and time as the flux from the source propagates.

In order to apply the output of the code to the X-ray data, we needed to transform the output to be readily compared to $N_{\rm H}$ under the assumption that all the material is cold (i.e., neutral; see Morrison & McCammon 1983). Within our formalism, this is equivalent to the approximation that the time- and frequency-dependent optical depth can be decomposed as $\tau(\nu, t) = N_{\rm H}\sigma(\nu)$, where $\sigma(\nu)$ is the average cross section at frequency ν weighed by the element abundance, and it is assumed to be independent of time, that is, independent of the ionization state of the elements[3]. We can then write the time-dependent column density in each observation band $[E_1, E_2]$ as

$$N_{\rm H} = N_{\rm H}(0)\left\langle \frac{\tau(\nu,t)}{\tau(\nu,0)} \right\rangle_{[E_1,E_2]}, \quad (1)$$

where the brackets indicate the average over the corresponding energy band.

We consider two types of environments, a wind (which can be expected for massive stars) and a uniform medium, the latter distributed between a minimum and a maximum radius. We varied the latter in the range $10^{18}\,{\rm cm} \le R_{\rm max} \le 10^{21}$ cm. For each value of $R_{\rm max}$, we then varied the minimum radius in the range $0.05 \le R_{\rm max}/R_{\rm min} \le 0.95$.

A wind-like density profile is described by $n(r) = n_0(r/r_0)^{-2}$. From a few test runs, we were able to immediately establish that a wind profile, even with extreme values of the initial column density $N_{\rm H}(0) = 10^{25}$ cm^{-2}, is ruled out by the data since in a wind most of the absorbing material is concentrated close to the source, and hence a sizable change in $N_{\rm H}$ happens on a very short timescale. Therefore, we focused our analysis on a uniform medium. The setup is such that it includes both the cases of a typical, extended interstellar medium and that of a thin shell, as envisaged in some models for GRB progenitors (Vietri & Stella 1998). For each combination of radii, the number density of neutral material prior to the burst onset is then given by $n = N_{\rm H}(0)/(R_{\rm max} - R_{\rm min})$.

We performed a Markov chain Monte Carlo (MCMC) analysis to determine the preferred values of $N_{\rm H}(t = 0)$ and $R_{\rm max}$. The results are shown in the upper panel of Fig. 3. The corresponding best fit is displayed in the bottom panel. As is visually evident, and formalized by a reduced $\chi^2_{\rm red} \sim 5$ (with eight degrees of freedom), a photoionization model is not a good explanation for the observed column density variability. The L-shaped isocontours in the corner plot reflect the fact that a constant value of absorption (the vertical part of the "L": $N_{\rm H} \sim 7 \times 10^{22}$ cm^{-2}, $R_{\rm max} > 5 \times 10^{19}$ cm) provides only a slightly worse fit than the case of a higher initial column at lower radii that is progressively eroded by photoionization (the horizontal part of the L, also shown in the bottom panel of Fig. 3). From a physical point of view, this result can be understood in light of the fact that photoionization is most effective during the early times, when the source is brighter. Hence, the model predicts an early decline, while the data show it at later times, when the flux is much weaker. Additional strain with the data is caused by the fact that a late decay of the column density is better explained if the absorber is confined within a very thin shell. At the same

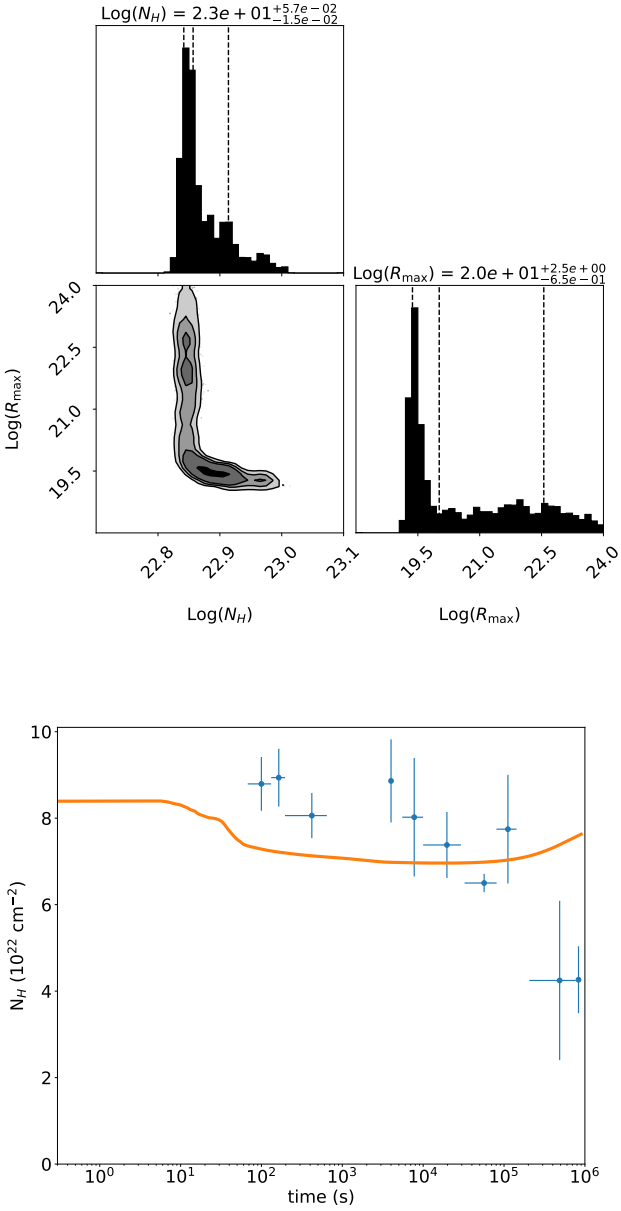

Fig. 3. Results of the photoionization code fit of the column density evolution with time. *Top*: results from the MCMC simulation for modeling via time-dependent photo-absorption. *Bottom*: corresponding best fit model from photo-absorption. The large $\chi^2_{\rm red} \sim 5$ shows that time-dependent absorption is not a good explanation for the observed time-variable absorption.

[3] This approximation is equivalent to assuming that the composition and temperature of the absorbing gas do not change with time. The same assumption was made in fitting the data with the `ztbabs` package for X-ray absorption.

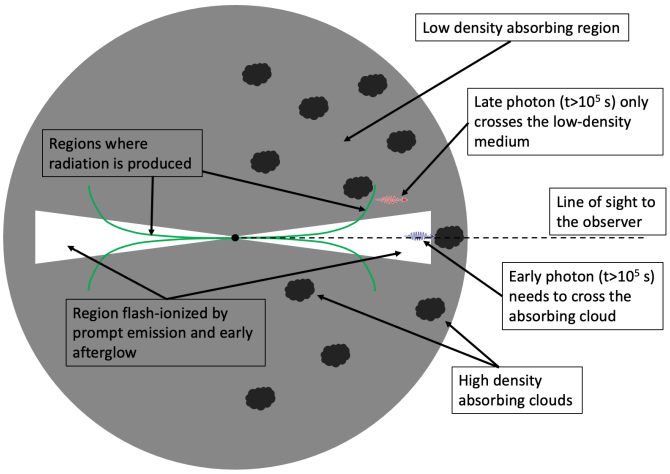

Fig. 4. Cartoon of the geometry for explaining a change of absorbing medium coincident with the observed jet break time. Early photons are produced close to the line of sight and need to cross the dense cloud that happens to lie along the line of sight and outside of the flash ionization cone. Late photons are produced at wider angles and travel toward the observer without crossing the high density cloud.

time, such a configuration implies a very high density medium, in which recombination is relatively fast. Recombination of free electrons onto ions is, as a matter of fact, the reason for the increase in column density observed at late times in Fig. 3. We conclude that time-dependent photo-absorption is not a good explanation for the observed $N_{\rm H}$ variability. In the following, we discuss some alternative explanations.

The MCMC fit for the time-dependent photoionization model includes any local absorber. We attempted a constant density absorber out to a radius $R_{\rm max}$ as well as a geometrically thin absorber located at a distance $R_{\rm max}$ from the burst. The former would reproduce, for example, the local molecular cloud within which the progenitor was born; the latter would instead include the edge of a cavity formed around the progenitor (e.g., an HII region such as in Watson et al. 2013 or a wind termination shock) as well as a physically unconnected cloud that happens to lie along our line of sight to the burst. We find that the geometrically thin absorber (shown in Fig. 3) gives a superior fit with respect to the uniform absorber. However, neither gives an acceptable fit, hence excluding the possibility that time-dependent photoionization of a relatively nearby absorber can explain the measured variable, $N_{\rm H}$. While a distant absorber could explain the overall large measured column density, it would not explain the observed decrease in the column density at late times.

4. Alternative explanations for the observed time-dependent absorption

Alternative explanations for the drop in the absorbing column at late times ($t \gtrsim 10^5$ s) require a real change of the column along the line of sight (irrespective of the gas ionization status). This can be due to a time evolution of the ambient medium, to a change of the line of sight, or a combination of the two. Interestingly, we note that the time of the drop in the absorbing column coincides with the estimated jet break time (Fraija et al. 2019).

In the case of a time-evolving absorber, we can envisage a medium with clouds or filaments with different densities. It should be kept in mind that the change in absorbing column is on the order of a factor of two, and, as a consequence, a moderate density contrast would suffice. If such clouds move, they might exit the line of sight to the burst at $t \sim 10^5$ s, when the absorbing column drops. Given the properties of GRB 190114C, it is possible to estimate the size of the emitting region at $t \sim 10^5$ s as (Derishev & Piran 2019)

$$r_{\perp,\rm obs} = R_{fb}/\Gamma = \left(\frac{6E_{\rm iso}t}{\pi n m_p c \Gamma^4}\right)^{1/4} \sim 2.6\times10^{17}\ {\rm cm} \quad (2)$$

for a uniform interstellar medium of density $n = 1$ cm^{-3} and using $E_{\rm iso} = 10^{54}$ erg. The Lorentz factor Γ is given by

$$\Gamma = \frac{1}{2}\left(\frac{3E_{\rm iso}}{8\pi n m_p c^5 t^3}\right)^{1/8}. \quad (3)$$

The absorbing cloud would need to have a size comparable to the emitting region and to have moved a distance comparable to its own size in a time $t_{\rm obs} \sim t_{\rm obs}\Gamma^2 \sim 1$ year. Such movement would require a speed comparable to the speed of light (~0.3 c), making this model highly unlikely.

Alternatively, one can consider that as time passes the fireball expands and so too does the bright ring from which most of the afterglow radiation is produced (Panaitescu & Mészáros 1998). If the absorber were to be porous, with a <1 surface filling factor and a coherence length comparable to the ring size, moderate variations in the absorbing column would be expected. This scenario is sketched in Fig. 4. The succession of events would be the following. Initially, the fireball flash ionizes a cone within the absorbing cloud of half opening angle equal to the jet angle, $\theta_j \sim 7.5°$, which we computed from the fireball properties listed above, with the estimated jet break time, $t_j = 10^5$ s (Fraija et al. 2019), and assuming a uniform unit density ambient medium. From the flash ionization runs described above, we know that the cone extends out to approximately 3×10^{19} cm. At the jet break time we observe a steepening in the light curve decay that we know is due to the fact that the fireball has now expanded sideways outside the original opening angle (Rhoads 1999), and therefore outside of the flash-ionized cone. It is therefore possible that from that time onward the radiation crosses an absorber with different properties. For a uniform absorber, we should observe a higher column density for $t > t_j$. In the case of GRB 190114C, we observe a drop in the column density. As a consequence, we need to invoke a clumped absorber, with a denser clump along the line of sight surrounded by a lower-density gas (see the sketch in Fig. 4). The observed coincidence of the jet break time with the change in absorbing column is definitively suggestive within this interpretation.

5. Summary and conclusions

We have presented X-ray observations of GRB 190114C, from several tens of seconds to about 10 days. We find that during the observing time window the absorbing column to the source decreases by a factor of about two. A statistical analysis with a time-dependent absorption model shows that the variability cannot be well modeled as the result of photo-absorption of the medium along the line of sight by the source photons. This result stems from the fact that the drop in the magnitude of $N_{\rm H}$ is observed at later times, after the most intense radiation has already passed through the medium. Any absorber that is close to the burst would be quickly photoionized, and the observed column would decrease in the first few tens of seconds. Any absorber that is far from the burst would produce constant

absorption. We could not find any configuration for which a progressively photoionized absorber can explain the late drop in the column density without an early, faster drop.

With the most straightforward interpretation not being supported by the data, we speculate on other possible physical mechanisms that may induce it. In particular, we argue that an absorber with a low filling fraction can produce such an effect, and we derive the required properties of the absorber. The typical dimensions of the absorbing blobs are those of Eq. (2), ∼0.1 pc. These are the typical sizes of ultra-compact HII regions or massive cores in molecular clouds.

One may also wonder why only a few GRBs showed changes in the absorbing column density. From an observational basis, time-dependent variable absorption is difficult to detect. Several high signal-to-noise X-ray spectra are needed, and these are not always available. A late-time decrease (or increase[4]) is even more difficult to detect as it requires good spectral data while the afterglow fades.

Another peculiarity of GRB 190114C is its connection with TeV emission. After the MAGIC detection (MAGIC Collaboration 2019b), two other firm GRB detections at TeV energies were made: GRB 190829A (de Naurois & HESS Collaboration 2019) at $z = 0.08$ (Valeev et al. 2019), detected by HESS, and GRB 201216C (Blanch et al. 2020) possibly at $z = 1.10$ (Vielfaure et al. 2020), detected by MAGIC. GRB 180720B at $z = 0.65$ (Vreeswijk et al. 2018) also showed very high energy photons that were detected by HESS (Abdalla et al. 2019). However, this emission came late (∼11 h).

GRB 190829A was a bright burst, but due to its proximity the overall energy was small, $E_{\rm iso} \sim 2 \times 10^{50}$ erg, and so was its peak luminosity (Tsvetkova et al. 2019). The burst was characterized by a high intrinsic column density ($N_{\rm H} \sim 2 \times 10^{22}$ cm^{-2}), which showed signs of a slight decrease of ∼40% within 10 ks. GRB 201216C was also a bright burst, $E_{\rm iso} \sim 6 \times 10^{53}$ erg (Frederiks et al. 2020), with a high intrinsic column density of $\sim 4 \times 10^{22}$ cm^{-2}. Even though the *Swift* data span only a very narrow time interval (3–15 ks after the GRB onset), there is an indication of a column density decrease by a factor of 4.0 ± 2.5. For both bursts, there was no *Fermi*/LAT detection. It is tempting to consider the high intrinsic column density as a common property of the TeV-emitting high- and low-luminosity GRBs. Such a connection may be due to the fact that the TeV emission is likely coming from the external shock and a high density of the external material would affect both the absorbing column and the afterglow properties. The reason for a correlation between TeV emission and column variability is, however, more difficult to anticipate, and a more detailed study is required make such a determination.

Acknowledgements. The authors would like to thank the anonymous referee for their comments and suggestions which helped improving the quality of the manuscript. SC acknowledges support from the Italian Space Agency, contract ASI/INAF n. I/004/11/4. SC warmly thanks the *XMM-Newton* Project Scientist, Norbert Schartel, for approving Director's Discretionary Time observations. RP acknowledges support by NSF award AST-2006839 and from NASA (Fermi) award 80NSSC20K1570. DL acknowledges support from NASA grant NNX17AK42G (ATP) and NSF grant AST-1907955.

[4] Ideally, if a blob enters the line of sight of the jet as the jet spreads out, one should observe an increase in the absorbing column density. This effect is possible but is even more difficult to observe. This is because, as the blob enters the jet line of sight, only a fraction of the jet-emitting area is affected, thus producing a small (partial) increase in $N_{\rm H}$.

References

Abdalla, H., Adam, R., Aharonian, F., et al. 2019, Nature, 575, 464
Ajello, M., Arimoto, M., Axelsson, M., et al. 2020, ApJ, 890, 9
Arcodia, R., Campana, S., Salvaterra, R., & Ghisellini, G. 2018, A&A, 616, A170
Behar, E., Dado, S., Dar, A., & Laor, A. 2011, ApJ, 734, 26
Belczynski, K., Perna, R., Bulik, T., et al. 2006, ApJ, 648, 1110
Berger, E., Price, P. A., Cenko, S. B., et al. 2005, Nature, 438, 988
Blanch, O., Longo, F., Berti, A., et al. 2020, GRB Coord. Network, 29075, 1
Böttcher, M., Dermer, C. D., Crider, A. W., & Liang, E. P. 1999, A&A, 343, 111
Campana, S., Romano, P., Covino, S., et al. 2006, A&A, 449, 61
Campana, S., Lazzati, D., Ripamonti, E., et al. 2007, ApJ, 654, L17
Campana, S., Salvaterra, R., Melandri, A., et al. 2012, MNRAS, 421, 1697
Campana, S., Salvaterra, R., Ferrara, A., & Pallottini, A. 2015, A&A, 575, A43
Cash, W. 1979, ApJ, 228, 939
Dalton, T., & Morris, S. L. 2020, MNRAS, 495, 2342
D'Elia, V., Fiore, F., Meurs, E. J. A., et al. 2007, A&A, 467, 629
D'Elia, V., Fiore, F., Perna, R., et al. 2009, A&A, 503, 437
de Naurois, M., & HESS Collaboration 2019, GRB Coord. Network, 25566, 1
de Ugarte Postigo, A., Thöne, C. C., Martín, S., et al. 2020, A&A, 633, A68
Derishev, E., & Piran, T. 2019, ApJ, 880, L27
Dessauges-Zavadsky, M., Chen, H.-W., Prochaska, J. X., Bloom, J. S., & Barth, A. J. 2006, ApJ, 648, L89
Evans, P. A., Beardmore, A. P., Page, K. L., et al. 2009, MNRAS, 397, 1177
Fraija, N., Dichiara, S., Pedreira, A. C. C. d. E. S., et al. 2019, ApJ, 879, L26
Frederiks, D., Golenetskii, S., Aptekar, R., et al. 2020, GRB Coord. Network, 29084, 1
Frontera, F., Amati, L., Lazzati, D., et al. 2004, ApJ, 614, 301
Fryer, C. L., Rockefeller, G., & Young, P. A. 2006, ApJ, 647, 1269
Galama, T. J., & Wijers, R. A. M. J. 2001, ApJ, 549, L209
Gehrels, N., Chincarini, G., Giommi, P., et al. 2004, ApJ, 611, 1005
Gendre, B., Corsi, A., & Piro, L. 2006, A&A, 455, 803
Gropp, J. D., Kennea, J. A., Klingler, N. J., et al. 2019, GRB Coord. Network, 23688, 1
Grupe, D., Burrows, D. N., Wu, X.-F., et al. 2010, ApJ, 711, 1008
Hjorth, J., Sollerman, J., Møller, P., et al. 2003, Nature, 423, 847
Hjorth, J., Malesani, D., Jakobsson, P., et al. 2012, ApJ, 756, 187
Krühler, T., Malesani, D., Fynbo, J. P. U., et al. 2015, A&A, 581, A125
Lazzati, D., & Perna, R. 2002, MNRAS, 330, 383
Lazzati, D., Perna, R., & Ghisellini, G. 2001, MNRAS, 325, L19
MAGIC Collaboration (Acciari, V. A., et al.) 2019a, Nature, 575, 455
MAGIC Collaboration (Acciari, V. A., et al.) 2019b, Nature, 575, 459
Mirabal, N., Halpern, J. P., Kulkarni, S. R., et al. 2002, ApJ, 578, 818
Mirabal, N., Halpern, J. P., Chornock, R., et al. 2003, ApJ, 595, 935
Morrison, R., & McCammon, D. 1983, ApJ, 270, 119
Panaitescu, A., & Kumar, P. 2000, ApJ, 543, 66
Panaitescu, A., & Mészáros, P. 1998, ApJ, 493, L31
Perley, D. A., Krühler, T., Schulze, S., et al. 2016, ApJ, 817, 7
Perna, R., & Lazzati, D. 2002, ApJ, 580, 261
Perna, R., & Loeb, A. 1998, ApJ, 501, 467
Perna, R., Lazzati, D., & Fiore, F. 2003, ApJ, 585, 775
Racusin, J. L., Karpov, S. V., Sokolowski, M., et al. 2008, Nature, 455, 183
Ravasio, M. E., Oganesyan, G., Salafia, O. S., et al. 2019, A&A, 626, A12
Reichart, D. E., & Price, P. A. 2002, ApJ, 565, 174
Rhoads, J. E. 1999, ApJ, 525, 737
Schady, P., Mason, K. O., Page, M. J., et al. 2007, MNRAS, 377, 273
Selsing, J., Fynbo, J. P. U., Heintz, K. E., & Watson, D. 2019, GRB Coord. Network, 23695, 1
Stanek, K. Z., Matheson, T., Garnavich, P. M., et al. 2003, ApJ, 591, L17
Starling, R. L. C., Willingale, R., Tanvir, N. R., et al. 2013, MNRAS, 431, 3159
Stratta, G., Fiore, F., Antonelli, L. A., Piro, L., & De Pasquale, M. 2004, ApJ, 608, 846
Thöne, C. C., Campana, S., Lazzati, D., et al. 2011, MNRAS, 414, 479
Tsvetkova, A., Golenetskii, S., Aptekar, R., et al. 2019, GRB Coord. Network, 25660, 1
Valeev, A. F., Castro-Tirado, A. J., Hu, Y. D., et al. 2019, GRB Coord. Network, 25565, 1
Vergani, S. D., Salvaterra, R., Japelj, J., et al. 2015, A&A, 581, A102
Vielfaure, J. B., Izzo, L., Xu, D., et al. 2020, GRB Coord. Network, 29077, 1
Vietri, M., & Stella, L. 1998, ApJ, 507, L45
Vreeswijk, P. M., Kann, D. A., Heintz, K. E., et al. 2018, GRB Coord. Network, 22996, 1
Watson, D., Zafar, T., Andersen, A. C., et al. 2013, ApJ, 768, 23
Willingale, R., Starling, R. L. C., Beardmore, A. P., Tanvir, N. R., & O'Brien, P. T. 2013, MNRAS, 431, 394